Ascidian-inspired soft robots that can crawl, tumble, and pick-and-place objects

Shirong Zheng[1], Tongil Park[2], Manh Cuong Hoang[1], Gwangjun Go[1], Chang-sei Kim[1,2], Jong-Oh Park[1,2], Eunpyo Choi[1,2], and Ayoung Hong[3]

***Abstract*— A cylindrical shaped marine invertebrate ascidian has muscle fibers surrounding its body, which induce the contraction motion when the animal senses the external stimuli. As inspired by its cylindrical shape and the contraction motion of the ascidian, we introduce a soft robot that resembles this water animal. In this letter, we first discuss the design of the robot that can be magnetically actuated and create different motions due to different magnetic moments for each segment of the robot. The crawling motion of the robot is presented with a sinusoidal waveform of the magnetic field and we demonstrate the utility of our bio-inspired soft robot for transporting a millimeter-sized object and releasing a drug in a specific location.**

I. Introduction

Living creatures have survived by adapting their shapes and behaviors for many thousands of years in nature, therefore their way of living and moving is extremely stabilized. Therefore, bio-inspired soft robots are widely investigated in recent years and they have exhibited different motions inspired by different living animals: crawling on a plate by millipede [1] or crawling in a tube by snake [2], floating and swimming on water by frog [3], rolling on a plate [4] and tumbling the whole body by dung beetle [5], and climbing a vertical surface by gecko [6], [7].

For soft robots to imitate and represent the locomotion of the living animals, the appropriate actuation methods are essential. Baiens *et al.* presented a soft robot actuated using an air pressure as a control input [8]. By changing the design of the internal passageway of the robot and combinations, they could achieve robot deformation and movement. Palagi *et al.* presented a swimming soft robot using a light field as a control input [9]. A periodic light pattern travels from one side to the other side of the robot and deforms the body

*This work was supported by the grant of the Korea Health Technology R&D Project through the Korea Health Industry Development Institute (KHIDI), funded by the Ministry of Health and Welfare, Republic of Korea (grant number: HI19C0642) and in part by the National Research Foundation of Korea (NRF) grant funded by the Korea government (MSIT) (No. 2020R1F1A1072201).

[1]S. Zheng, M. C. Hoang, G. Go, C.-S. Kim, J.-O. Park, and E. Choi are with the School of Mechanical Engineering, Chonnam National University, Gwangju, South Korea seyeongj33@gmail.com, hmcuong.hust@gmail.com, gwangjun124@gmail.com, ckim@jnu.ac.kr, jop@jnu.ac.kr, eunpyochoi@jnu.ac.kr

[2]T. Park, C.-S. Kim, J.-O. Park, and E. Choi are with the Korea Institute of Medical Microrobotics, Gwangju, South Korea. tongil.park@kimiro.re.kr

[3]A. Hong is with the Robotics Engineering Convergence and the Department of AI Convergence, Chonnam National University, Gwangju, South Korea. ahong@jnu.ac.kr

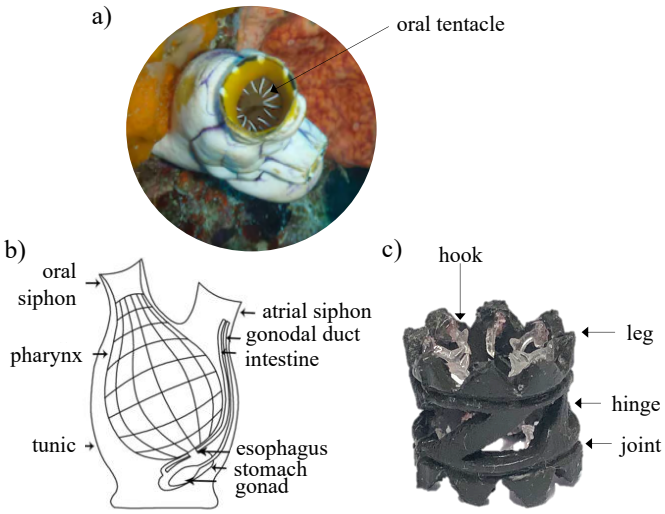

Fig. 1. A magnetically controlled soft robot inspired by the water animal, ascidian. (a) The picture and (b) the anatomy of ascidian. (c) The fabricated ascidian-inspired soft robot. (Images obtained and adapted from [13] and ©Shutterstock images, courtesy of Jesus Cobaleda.)

shape. The magnetic actuation has been combined with other actuation methods to control soft structures. For example, the magnetic system controls the movement of the robot while the temperature change induces the deformation of the soft robot body [10], [11], and controls the orientation of the robot while the acoustic transducer generates speed [12].

These magnetically actuated soft robots mostly consist of a soft structure embedded with soft or permanent magnetic particles inside [14]–[16]. As the structure is exposed to the magnetic field, the soft magnetic particles align with the external magnetic field and create chains so that the soft robot could have a magnetic easy axis. Compared to the soft magnetic particles, permanent magnetic particles have a higher magnetic remanence that contributes to the deformation of the soft robot. However, the permanent magnetic particles require a higher magnetic field on the magnetization process.

Different methods have been proposed to fabricate the magnetic soft robots. Venkiteswaran *et al.* attached the magnetic particles embedded silicon rubber to the pure silicon rubber and presented four different types of bio-inspired soft robots [17]. Song *et al.* used permanent magnetic powders and reprogrammed their magnetic properties using a strong magnetic field during magnetization [18]. Xu *et al.* and Du *et al.* used UV-curing method with a file mask to obtain the

complex shape of the robot with different magnetization directions [16], [19]. However, these methods were limited to a planar structure. Lee *et al.* and Gervasoni *et al.* recently presented a 3D printing technique to fabricate robots in two- and three-dimensions [20], [21]. They fabricated the robots as a single strip which limits the motion of the robot.

In this letter, we present a new millimeter-scale soft robot inspired by the shape and the motion of the water animal, ascidian (see Fig. 1). The three-dimensional cylindrical shape of the soft robot is fabricated using the molding technique without assembling. The segments of the fabricated soft robot were magnetized in a different direction at one step by deforming the structure in a specific shape. The soft robot is fabricated with the silicone rubber and the permanent magnetic particles and shows different motions and functions by designing the direction of the magnetic moment different for each part of the robot. The crawling motion was examined with a specific waveform magnetic input by deforming the full-body structure. Finally, we demonstrate that the presented soft robot can perform a pick-and-place task and a drug-release task in millimeter scale.

II. Ascidian-inspired Soft Robot Design

A. Robot design

Ascidian, also called a sea squirt, is a cylindrical invertebrate animal mostly living in shallow water as shown in Fig. 1 (a). The body of the ascidian is surrounded by a tunic that may be thin, delicate, transparent, and gelatinous. The ascidian also have two openings, such as oral and atrial siphon, where the water flows in and out, as shown in Fig. 1 (b).

The initial design of our soft robot is inspired by the self-protection mechanism of the marine invertebrate, ascidian. When this animal senses the external stimuli, the muscle surrounding its body contracts and squeezes out the water kept in its body. To mimic the contraction motion of the ascidian, we designed the cylindrical soft robot including four hinges on its circular side as shown in Fig. 1 (c). The hinges which are magnetized in a certain direction will have their own magnetic moments; when they are exposed to the external magnetic field they align to the direction of the field. Therefore, the robot can twist its body and shorten its length as it is magnetically actuated. The ascidian has tentacles inside the oral siphon which are usually used for grasping and feeding as shown in Fig. 1 (a). Inspired by this structure, the hook was designed and attached to the inside of the legs. It has two sharp corners that could pierce the trapped materials inside the robot by repeating the opening and closing motion of the legs.

Although most ascidians are attached to the substrate and remained in the fixed location for their life cycles, we designed the soft robot able to move in a specific environment [22]. We added eight legs at each side of the robot, inspired by the motion of the oral and atrial siphon of the ascidian. Depending on the magnetic moment of the legs, we can control the motion of them (i.e., open or closed) when exposed to the external magnetic field.

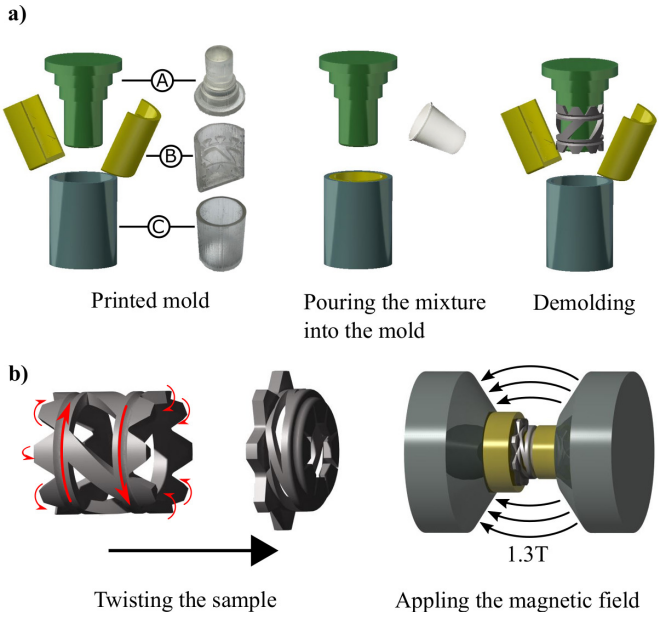

Fig. 2. A fabrication and magnetization process of a soft robot. (a) The mold consists of four main components; one inner-cylinder (Ⓐ), two truncated cylinders with the pattern engraved inside (Ⓑ) and one outer-cylinder (Ⓒ). The mixture of silicon and permanent magnetic particles are poured into the printed mold and demolded after curing. (b) The fabricated soft robot is magnetized with a magnetic field magnitude of 1.3 T while it is twisted to the red direction.

The designed soft robot was magnetized in two different configurations. One was designed to have the same magnetic moments for the legs at both sides. This creates the opposite opening and closing motion of the legs. The contraction motion of the hinges combining with the leg motion help the robot crawl in a constrained environment. The other was designed to have the opposite direction of the magnetic moments for the legs on both sides. This generates the legs closing simultaneously and therefore robot can grab and transport objects. We also designed joints between the legs and the body parts to ease the opening and closing motion of the legs.

B. Fabrication of the robot

1) Materials: We used the neodymium-iron-boron particles (NdFeB, from Neo Magnequench, Canada) with a mean size of 5 μm as a magnetic material in this paper. The unmagnetized particles with a magnetic remanence of 891 mT was utilized and magnetized after the robot is fabricated. We used silicone rubber (Ecoflex 0020, Smooth-On, Inc,. USA) to form a soft part of the robot. The utilized material has the tensile strength of 160 psi and the elongation at break of 845 %, which provides a good strength and ductility for the robot body.

2) Fabrication: We fabricated a soft robot with a molding technique as shown in Fig. 2 (a). We designed the mold with four components; one inner-cylinder, two truncated cylinders with the pattern engraved inside, and one outer-cylinder. The shape of the soft robot was patterned at inside surface of the truncated cylindrical molds. The space between two of

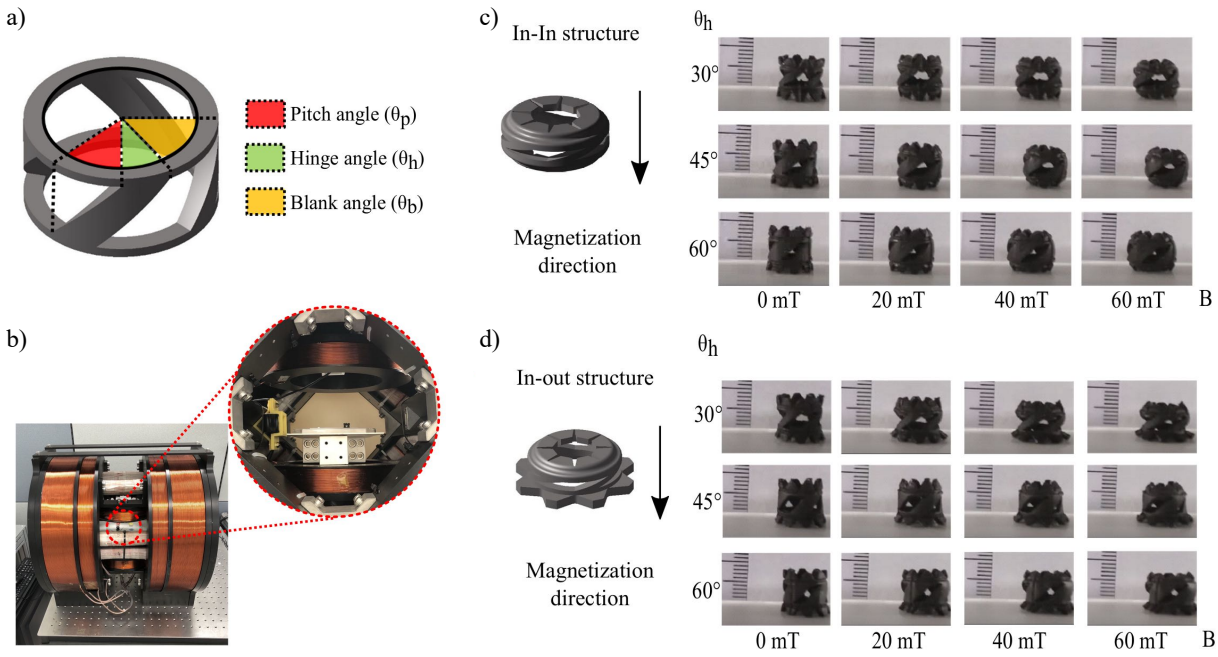

Fig. 3. The deformation of the soft robot under the magnetic field. (a) The structure of the soft robot with design parameters: pitch angle (θ_p), hinge angle (θ_h), and blank angle (θ_b). (b) The EMA system with a closer look at the workspace. The deformation of the (c) in-in structured robot and (d) in-out structured robot with respect to the hinge angle (θ_h) and the magnitude of the magnetic field.

those molds and the inner cylinder was later filled with the mixture. The outer cylindrical mold was used for maintaining molds. The designed mold was fabricated using a 3D printer (Objective Eden260V, Stratasys, USA) and coated with a thin layer of release agents (Ease release 200, Smooth-on, Inc., USA) which prevents adhesion between the mold and the created soft robot.

The silicone rubber and the magnetic particles were mixed in a mass ratio of 1:1. The mixture was first stirred and placed in a vacuum pump for 3 minutes to eliminate bubbles, poured into the prepared mold, and cured in the oven at 70 ° for 4 hours. The fabricated soft robot has a height of 10 mm, an outer diameter of 10 mm, a thickness of 1 mm, and a leg length of 2 mm.

3) Magnetization: We used a vibrating sample magnetometer (VSM) to magnetize the permanent magnetic particles embedded in the robot [23]. To control the magnetization direction of each part in the soft robot, we kept the soft robot in a certain configuration while it was magnetized as shown in Fig. 2 (b). The main body of the soft robot was twisted and the gap between hinges was narrowed as long as they were not overlapped. The legs on both sides were folded in or out as we designed. To magnetize the soft robot, we applied the magnetic field with a magnitude of 1.3 T which is larger than the remanence of the magnetic particles.

C. Deformation under actuation

The deformation of the fabricated soft robot was first tested under the simple uniform magnetic field as shown in Fig. 3. To examine the contribution of the hinges to the contraction motion, we fabricated soft robots with different hinge angles as $\theta_h = \{30,\ 45,\ 60\}^\circ$. This determines the width of the hinge as $w_h \approx r\theta_h$ where r is the radius of the soft robot. The sum of the blank angle (θ_b) and the hinge angle (θ_h) was maintained to 90° by evenly spacing four hinges to each other. The pitch angle was remained constant as 45°; this value was experimentally chosen to maximize the magnetic torque exerted on the hinge. By increasing the strength of the external magnetic field from 0 mT to 60 mT, we observed that the body of the robot exhibited different displacement of twisting motion. We selected the robot designed with the hinge angle of 30° for further experiments since it showed the largest deformation. We have investigated the portion of the fully magnetized volume within the hinge and its magnetization direction for three different robots. The robot with the hinge angle of 30° supposed to have a largest deformation under the uniform magnetic field.

The legs of the soft robot were magnetized in two different configurations as discussed in section II. The legs of the in-in structured robot bent inward as it is exposed to the magnetic field as shown in Fig. 3 (c). For the in-out structured robot, the upper legs bent inward and the lower bent outward as shown in Fig. 3 (d). The robot legs for both types were aligned better with the magnetic field direction as its magnitude increased, however, the effect of the hinge angle was not noticeable for the leg motion.

III. Experimental Demonstration

A. Experimental setup

1) Manipulation system: We utilized the external electromagnetic actuation (EMA) system with one pair of Maxwell coils, a pair of Helmholtz coils, and two pairs of rectangular coils, as described in Fig. 3 (b) [24]. The system can accom-

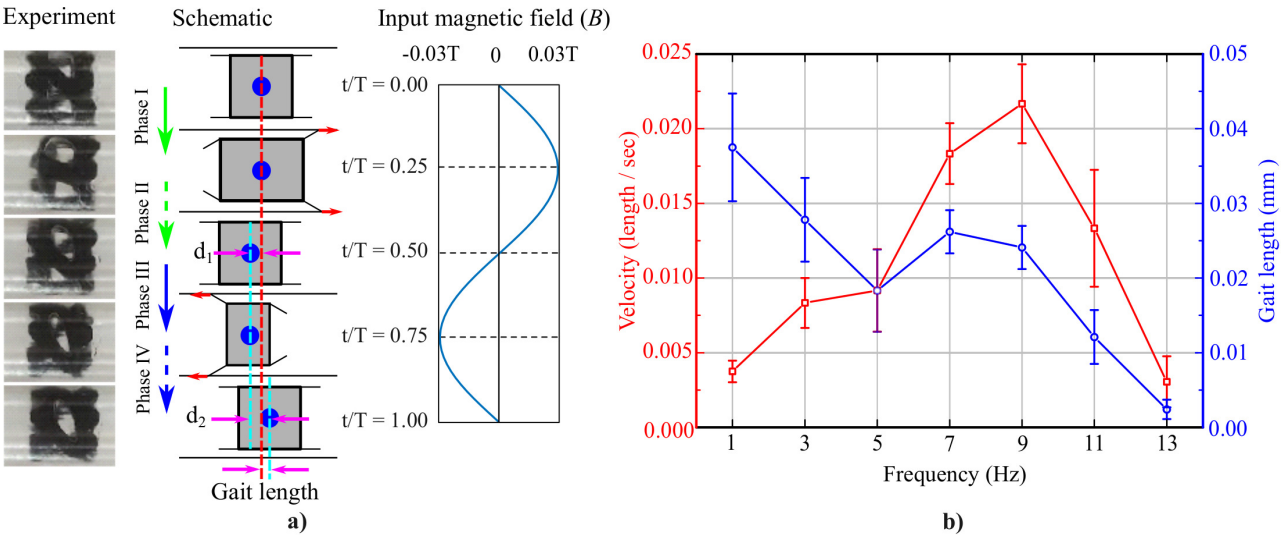

Fig. 4. Experiment demonstration of the ascidian-inspired soft robot crawling in a plastic tube under the magnetic input as the sinusoidal periodic waveform $B = A\sin(2\pi ft)$. (a) The schematic diagram of the crawling gait along with the captured images and the exerted sinusoidal input magnetic field. Each step of the schematic diagram corresponds to the input wave of each stage. (b) The velocity normalized to the body length (red) and the gait length (blue) of the soft robot as a function of the frequency of the sinusoidal magnetic field input.

modate for magnetic fields of up to 35 mT and its magnetic workspace is a 60 mm×60 mm×60 mm at the center of a coil configuration. The EMA system were controlled by eight power suppliers consist of four NX15 units and four 3001iX units (AMETEK, USA) and run by a LabVIEW program.

2) Drug-loaded capsule model: To demonstrate the controlled drug release by using the presented soft robot, we prepared the model of a drug-loaded capsule. [25] The Ooho edible water capsule was used as the model and its fabrication process was as follows: 1) melt 1 g of sodium alginate (Sigma Aldrich, St. Louis, USA) and 1 g of calcium chloride (Calcium L-lactate hydrate, Sigma Aldrich, St. Louis, USA) in the deionized (DI) water to prepare solutions for each, 2) stir the solutions until it all dissolves and sit for 15 minutes, 3) add 1 ml of red food color in the alginate solution, 4) immerse the fabricated soft robot in the calcium solution, 5) squeeze the red alginate solution about 300μl via a pipette to the space inside the soft robot, 6) sit for one minute to create a capsule membrane, and 7) lift the robot with the capsule inside and put it in the DI water.

We would like to note that the thickness of the membrane can be controlled by reaction time in the step 6 and it is important to determine the time since it can affect the subsequent drug release.

B. Crawling in the tube

We tested the crawling motion of the in-out structured robot in a plastic tube. The magnetic field with the varying magnitude but with the stationary direction was utilized in the experiment. The magnitude of the magnetic field was determined as $B = A\sin(2\pi ft)$ where A is the amplitude and f is the frequency of the input. The amplitude of the input sinusoidal wave was decided to 30 mT, which is comparable to the maximum field that can be accommodated with the EMA system.

The schematic drawing of the crawling gait is presented in Fig. 4 (a) with the captured experimental images of the soft robot (left) and the input waveform (right), corresponds to the schematics. In phase I, the magnetic field was increased in the opposite of the robot's magnetization direction. Due to the torque exerted on the hinge and leg segments, this actuation induced the untwisting motion of the robot body so that the body length increased and the anchorage of the front legs to the tube by bending outward. In phase II, the soft robot deformed back to its initial shape that generated a slight backward motion with a distance of d_1 because the front legs pushed the wall to the front. In phase III, the magnetic field was increased in the same direction to the robot's magnetization direction. Each part of the robot then tried to align its magnetic moment to the field and the shape of the robot became as it was magnetized. This induced the twisting (or contraction) motion of the robot body and the anchorage of the back legs. In phase IV, which is the final one in the cycle, the robot deformed again back to its initial shape as in phase II. However, here the back legs pushed the wall and generated a forward movement with a distance of d_2. The gait length (l) of this crawling motion is the total forward movement of the robot; i.e., the difference between the forward and backward movement as $l = d_2 - d_1$, which is related to the body length of the robot. The distance d_1 corresponds to the change of the body length when the robot is untwisted and stretched, and d_2 when the robot is twisted and contracted. Therefore, these distances d_1 and d_2 are the values determined by the pitch angle (θ_p) of the designed soft robot.

The crawling velocity normalized to the body length and the gait length of the soft robot was examined as a function of the input frequency as shown in Fig. 4 (b). We measured the displacement of the robot traveling for one minute along the

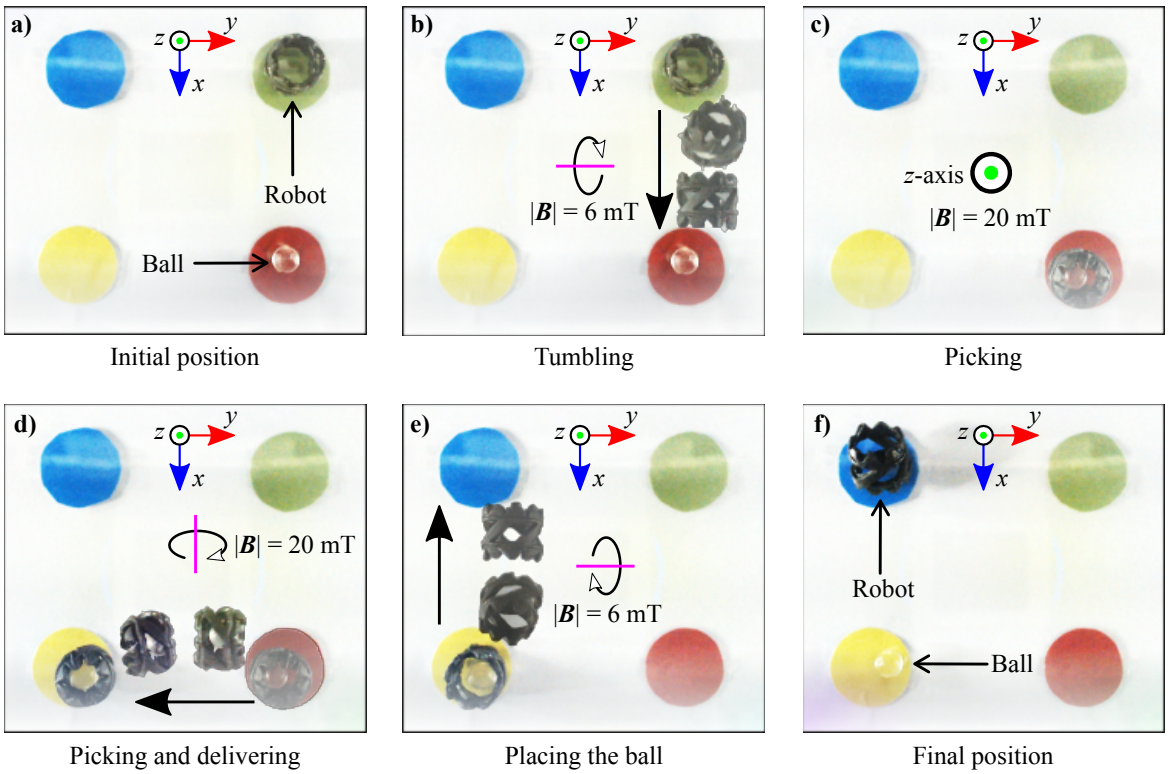

Fig. 5. Experimental demonstration of the ascidian-inspired soft robot on a pick-and-place task. The captured images show the robot (a) at its initial position on the green circle, (b) tumbling to reach and (c) picking the ball on the red circle, (d) tumbling to reach the yellow circle by carrying the ball, (e) placing the ball on the yellow circle and tumbling to the blue circle, and (f) on the blue circle after the pick-and-place task.

longitudinal axis of the tube to estimate the crawling velocity and the gait length. We repeated the experiment for five times for each input frequency ranging from 1 to 13 Hz. The crawling velocity tended to increase as the input frequency increased until 9 Hz where the robot reached the crawling velocity of 0.22 mm/s on average; which corresponds to about 0.022 bodylength/s. The largest gait length was obtained as 0.375 mm when the input frequency was 1 Hz and the length decreased as the input frequency increased. The input frequency may have reached the step-out frequency around 9 Hz so that the exerted magnetic torque is not strong enough to maintain the robot motion synchronized with the input field and the crawling velocity drastically declined. (Note that the scales of the graph for the crawling velocity and the gait length are different.)

The crawling motion of the robot was also examined with a different periodic input such as a square wave. However, the square wave could not create the net translational motion for the robot and sometimes the robot attempted to flip its body especially when the frequency was low. We inferred that the magnetized part of the robot were not able to follow the abrupt direction change of the magnetic field.

C. *Pick-and-place*

We used the in-in structured soft robot to demonstrate the pick-and-place task. Four points assigned with different colors were positioned on a plate as shown in Fig. 5. At the initial time, the soft robot was placed on the green circle and the 3D printed plastic ball as an object on the red circle, respectively. In this demonstration, the task for the robot is to pick up the ball on the red, transfer it to the yellow, and go to the blue. The operator controlled the orientation of the magnetic field input using a joystick.

The magnetic field rotating around the y-axis generated the tumbling motion of the robot (Fig. 5 b). As the robot approaches the plastic ball on the red, we adjusted the orientation of the robot with a joystick to trap the ball, then increased the magnitude of the magnetic field from 6 mT to 20 mT along the z-axis. Therefore, the legs on both sides of the robot are bent inward to trap the plastic ball (Fig. 5 c). As the robot completely encased the ball, the rotating magnetic field around the x-axis was applied to make robot reaching the yellow point (Fig. 5 d). As long as the robot reached the yellow point, the field magnitude was decreased to 6 mT along the z-axis that released the ball in the place. The rotating magnetic field around the y-axis generated the tumbling motion of the robot to the blue circle (Fig. 5 e). The robot on the last blue point after the pick-and-place task (Fig. 5 f). The magnetic field strength was increased/decreased gradually with a step of 1 mT to prevent undesired motion of the robot when the switching between the tumbling and picking is required.

D. *Drug-release*

The in-in structured robot with hooks attached inside the legs was used in the drug-release demonstration. The

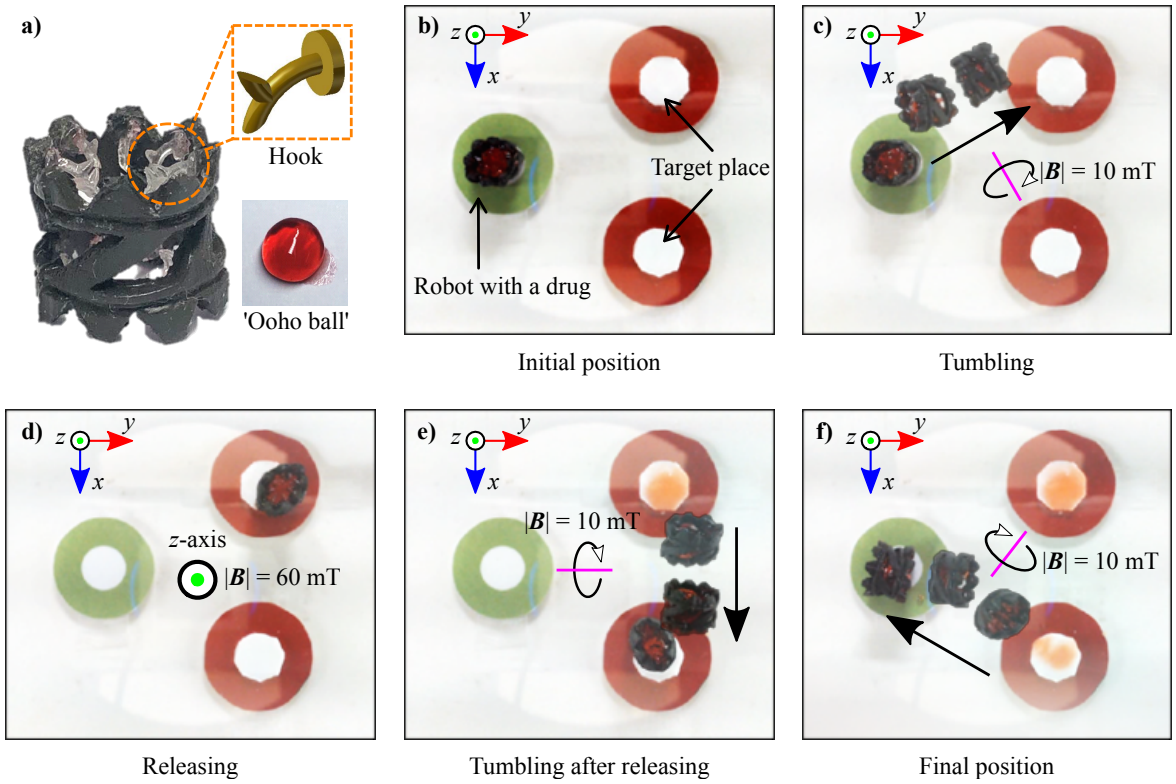

Fig. 6. Experimental demonstration of the ascidian-inspired soft robot on a drug-release task. (a) The fabricated robot with hooks bonded on the robot's legs and the 'Ooho' ball as the drug model. The captured images show the robot (b) at its initial position, (c) tumbling to reach the first releasing target, (d) releasing the drug by squeezing motion, (e) tumbling to reach the second releasing target, and (f) after the drug-release task.

orientation of the magnetic field input was also controlled by the operator using a joystick.

The task for drug-release demonstration is to release the drug model, which is already embedded in the soft robot, to the target regions and return to its initial position. At the initial time point, the soft robot was placed on the green point (Fig. 6 b). We controlled the rotating axis of the magnetic field with a magnitude of 10 mT that the robot could approach the first target region (Fig. 6 c). Then we increased the field strength to 60 mT to contract the hinge at the same time closing the legs. As repeatedly turning the magnetic field on and off, the hook attached on the legs kept damaging the membrane of the drug-loaded capsule model (Fig. 6 d). After the first release, the rotating magnetic field with the decreased magnitude of 10 mT was applied to create the tumbling motion of the soft robot and reach it to the second target region (Fig. 6 e). As the second drug release completed, the soft robot was brought back to its initial position using the decreased field strength (Fig. 6 f).

IV. Conclusion

In this letter, the ascidian-inspired soft robot is designed to create a different motion, such as crawling and tumbling, under the magnetic field actuation by means of the different magnetic moment for each robot segment. Despite many different designs and fabrication methods for magnetically actuated soft robots, peristaltic-like locomotion of magnetic soft robots with the full-body shape deformation is first demonstrated in this letter. The crawling motion was studied with the sinusoidal magnetic field waveform when the robot was constrained in the tube. We also demonstrated feasibility of using the presented soft robot for transporting objects and releasing drug in millimeter scale.

The presented soft robot combined with the EMA systems have many promising applications within the biomedical areas since the robot can be fabricated with bio-compatible materials and remotely actuated within the human body. The investigation on determining the optimal input that generates higher crawling speed and the intelligent control method that automatically loads and transports the drug to the target position would be our future work. Different sizes and shapes of the robot and drug model will be studied to improve the drug release effect.

References

[1] V. K. Venkiteswaran, D. K. Tan, and S. Misra, "Tandem actuation of legged locomotion and grasping manipulation in soft robots using magnetic fields," *Extreme Mech Lett*, p. 101023, 2020.

[2] J. Nam, S. Jeon, S. Kim, and G. Jang, "Crawling microrobot actuated by a magnetic navigation system in tubular environments," *Sens Actuators A Phys*, vol. 209, pp. 100–106, 2014.

[3] S. Miyashita, S. Guitron, M. Ludersdorfer, C. R. Sung, and D. Rus, "An untethered miniature origami robot that self-folds, walks, swims, and degrades," in *IEEE Int Conf Robot Autom*, pp. 1490–1496, IEEE, 2015.

[4] H.-W. Tung, K. E. Peyer, D. F. Sargent, and B. J. Nelson, "Noncontact manipulation using a transversely magnetized rolling robot," *Appl Phys Lett*, vol. 103, no. 11, p. 114101, 2013.

[5] C. Bi, M. Guix, B. V. Johnson, W. Jing, and D. J. Cappelleri, "Design of microscale magnetic tumbling robots for locomotion in multiple environments and complex terrains," *Micromachines*, vol. 9, no. 2, p. 68, 2018.

[6] S. Kim, M. Spenko, S. Trujillo, B. Heyneman, D. Santos, and M. R. Cutkosky, "Smooth vertical surface climbing with directional adhesion," *IEEE Trans Robot*, vol. 24, no. 1, pp. 65–74, 2008.

[7] G. Gu, J. Zou, R. Zhao, X. Zhao, and X. Zhu, "Soft wall-climbing robots," *Sci Robot*, vol. 3, no. 25, 2018.

[8] R. L. Baines, J. W. Booth, and R. Kramer-Bottiglio, "Rolling soft membrane-driven tensegrity robots," *IEEE Robot Autom Lett*, vol. 5, no. 4, pp. 6567–6574, 2020.

[9] S. Palagi, A. G. Mark, S. Y. Reigh, K. Melde, T. Qiu, H. Zeng, C. Parmeggiani, D. Martella, A. Sanchez-Castillo, N. Kapernaum, *et al.*, "Structured light enables biomimetic swimming and versatile locomotion of photoresponsive soft microrobots," *Nat Mater*, vol. 15, no. 6, pp. 647–653, 2016.

[10] H.-W. Huang, M. S. Sakar, A. J. Petruska, S. Pané, and B. J. Nelson, "Soft micromachines with programmable motility and morphology," *Nat Commun*, vol. 7, no. 1, p. 12263, 2016.

[11] G. Go, Z. Jin, J.-O. Park, S. Park, *et al.*, "A thermo-electromagnetically actuated microrobot for the targeted transport of therapeutic agents," *Int J Control Autom Syst*, vol. 16, no. 3, pp. 1341–1354, 2018.

[12] D. Ahmed, C. Dillinger, A. Hong, and B. J. Nelson, "Artificial Acousto-Magnetic Soft Microswimmers," *Adv Mater Technol*, vol. 2, p. 1700050, jul 2017.

[13] Royal BC Museum. Available at: http://taxonomy.royalbcmuseum.bc.ca/.

[14] S. Kim, F. Qiu, S. Kim, A. Ghanbari, C. Moon, L. Zhang, B. J. Nelson, and H. Choi, "Fabrication and characterization of magnetic microrobots for three-dimensional cell culture and targeted transportation," *Adv Mater*, vol. 25, no. 41, pp. 5863–5868, 2013.

[15] M. Medina-Sánchez, L. Schwarz, A. K. Meyer, F. Hebenstreit, and O. G. Schmidt, "Cellular cargo delivery: Toward assisted fertilization by sperm-carrying micromotors," *Nano Lett*, vol. 16, no. 1, pp. 555–561, 2016.

[16] T. Xu, J. Zhang, M. Salehizadeh, O. Onaizah, and E. Diller, "Millimeter-scale flexible robots with programmable three-dimensional magnetization and motions," *Sci Robot*, vol. 4, no. 29, 2019.

[17] V. K. Venkiteswaran, L. F. P. Samaniego, J. Sikorski, and S. Misra, "Bio-inspired terrestrial motion of magnetic soft millirobots," *IEEE Robot Autom Lett*, vol. 4, no. 2, pp. 1753–1759, 2019.

[18] H. Song, H. Lee, J. Lee, J. K. Choe, S. Lee, J. Y. Yi, S. Park, J.-W. Yoo, M. S. Kwon, and J. Kim, "Reprogrammable ferromagnetic domains for reconfigurable soft magnetic actuators," *Nano Lett*, 2020.

[19] X. Du, H. Cui, T. Xu, C. Huang, Y. Wang, Q. Zhao, Y. Xu, and X. Wu, "Reconfiguration, camouflage, and color-shifting for bioinspired adaptive hydrogel-based millirobots," *Adv Funct Mater*, vol. 30, no. 10, p. 1909202, 2020.

[20] S. Gervasoni, A. Terzopoulou, C. Franco, A. Veciana, N. Pedrini, J. T. Burri, C. de Marco, E. C. Siringil, X.-Z. Chen, B. J. Nelson, *et al.*, "Candybots: A new generation of 3d-printed sugar-based transient small-scale robots," *Adv Mater*, p. 2005652, 2020.

[21] H. Lee, Y. Jang, J. K. Choe, S. Lee, H. Song, J. P. Lee, N. Lone, and J. Kim, "3d-printed programmable tensegrity for soft robotics," *Sci Robot*, vol. 53, pp. 61–64, 2020.

[22] P. Bhovad, J. Kaufmann, and S. Li, "Peristaltic locomotion without digital controllers: Exploiting multi-stability in origami to coordinate robotic motion," *Extreme Mech Lett*, vol. 32, p. 100552, 2019.

[23] B. A. Darmawan, S. B. Lee, G. Go, K. T. Nguyen, H.-S. Lee, M. Nan, A. Hong, C.-S. Kim, H. Li, D. Bang, *et al.*, "Self-folded microrobot for active drug delivery and rapid ultrasound-triggered drug release," *Sens Actuators B Chem*, vol. 324, p. 128752, 2020.

[24] M. C. Hoang, K. T. Nguyen, V. H. Le, J. Kim, E. Choi, B. Kang, J.-O. Park, and C.-S. Kim, "Independent electromagnetic field control for practical approach to actively locomotive wireless capsule endoscope," *IEEE Trans Syst Man Cybern Syst*, 2019.

[25] H. H. Tønnesen and J. Karlsen, "Alginate in drug delivery systems," *Drug Dev Ind Pharm*, vol. 28, no. 6, pp. 621–630, 2002.